

22

Attosecond Time-Resolved Spectroscopy at Surfaces

Adrian L. Cavalieri, Ferenc Krausz, Ralph Ernstorfer, Reinhard Kienberger, Peter Feulner, Johannes V. Barth, and Dietrich Menzel

22.1

Overview

An area of physics exhibiting rapid progress and strongly focused interest is that of extremely fast phenomena; both the development of suitable methods and the understanding of such processes are at issue. While the term “ultrafast” was originally used for processes occurring in the (first upper, then lower) femtosecond range, today timescales of 1 fs or fractions thereof are accessible. This does not represent a marginal improvement, but encompasses a qualitative change: from the range where in principle the Born–Oppenheimer approximation, albeit with diabatic extensions, can be applied, to that of true nonadiabatic response, where the motion of individual electrons becomes the focus of attention. Therefore, the opportunity now exists to investigate the motions of electrons within many-electron systems, including the development of coupled many-body responses like the formation of band structure and the buildup of screening responses. First attempts to push into this range by looking at, for example, the ultrafast charge transfer at surfaces have been made successfully in the last 15 years with the core hole clock method. However, the latest developments utilizing attosecond laser pulses promise to provide a general tool to investigate in detail, and with few restrictions, this realm of electronic motions. While significant methodological development remains necessary for complete utilization and interpretation of measurements made on the attosecond timescale, the results obtained so far are extremely promising. It is timely, therefore, to give an overview of some past approaches, the most recent developments, and to identify the types of problems that should be attacked in the future using this exciting new tool. We will focus in particular on processes occurring at surfaces, because they contain *in nuce* the ingredients operative in atoms and molecules together with the important effects of solids.

With this contribution, a short overview of surface-relevant processes proceeding on the attosecond timescales will be given. In its first part, we present a selection of ultrafast phenomena and show how they can be accessed under continuous wave (cw) conditions, that is, in experiments where no temporal resolution is provided either by attosecond excitation pulses or by ultrafast detection. We use this part to introduce key phenomena of ultrafast dynamics on surfaces and to illustrate the limits of conventional methods. In the second part (Chapter 22.3), we demonstrate how the application of laser-based attosecond metrology can be used to overcome these limits.

22.2

Examples for Ultrafast Dynamics on Solid Surfaces

22.2.1

Electronic Response

When comparing electron binding energies from photoemission experiments on isolated atoms with one-electron energy levels of the unperturbed particle obtained from one-electron calculations, significant differences appear, which are larger for more localized and compact photoionized orbitals [1, 2]. This effect, known as intraatomic relaxation, is due to a rearrangement of the ion's electron distribution in response to the creation of the vacancy. As a result, the total energy of the ion is decreased and the kinetic energy of the photoelectron is increased. Coulombic and exchange energy also contribute to the observed increase in kinetic energy. For incomplete relaxation, part of the excess energy remains in the ion as a bound or continuum excitation, and additional shake-up or shake-off satellites are observed in addition to the main lines in the photoelectron spectrum [1, 3]. For molecules or solid compounds, this satellite structure can be very rich due to contributions of local and nonlocal excitations (e.g., plasmons) and charge transfer between the atomic constituents of the compound [1]. To gain perspective, we will examine a simple case: an atom adsorbed onto a surface that is photoionized. We assume that charge transfer is slow. In this case, only the polarization of the surrounding matrix will contribute the additional, extraatomic part to the total relaxation energy. It is largest for metallic substrates with delocalized conduction electrons (typically $\sim 1\text{--}2$ eV) and smallest for insulators with low ϵ [1, 4]. How fast does this simple screening process proceed (and all the other, more complicated processes mentioned above)? Calculations indicate that the dynamics can be divided into two parts: For *short* times, defined by less than one half of a plasma frequency oscillation period, the electrons react ballistically as independent particles. For *long* times, collective oscillations with the plasma frequency are encountered [5]. For all metals, these dynamics proceed in the sub-femtosecond regime due to their corresponding plasma frequencies. So far, time-resolved measurements have only been possible for semiconductors with very low electron density and correspondingly small plasma frequency [6]. Do cw experiments allow access to these dynamics? One could consider photoemission experiments on

identical atoms bound to different surfaces with very different plasma frequencies. Using different photon energies resulting in low and high kinetic photoelectron energies, that is, slow or fast photoelectron release, one could hope to see differences in the response of the matrix showing up as shifts of the experimentally obtained binding energies. Unfortunately, such an experiment fails. Due to the temporally extended photon pulses from conventional cw sources, the photoemission process will occur for a long time and the experimentally obtained spectrum will be dominated by the fully screened final state in both cases. Since the adiabatic limit is never reached, there will also be lines from less or unscreened final states even if the excitation process is extended by using extremely narrowband radiation [3]. The spectrum sums over all possible final states and for practical situations, it is always close to the sudden limit. Therefore, feasible cw approaches to screening dynamics are difficult.

One way to access the screening dynamics would be to monitor a process in which two electrons are emitted sequentially, separated by a time interval comparable to the critical screening time noted above. The analysis of postcollision interaction (PCI) line shapes [7] falls into this category and consequently seems promising. During PCI, near-threshold ionization of inner shell levels results in slow photoelectrons that are still within reach of the ion's Coulomb potential when the core hole decays by a subsequent Auger process. This doubles the ion's positive charge and increases the attractive force on the threshold photoelectron. Because of the statistical nature of core decay, broadened and red (blue) shifted energy profiles result for the photo (decay) electrons for such near-threshold ionization of core levels [7]. For an adsorbate on a surface, screening by extraatomic polarization reduces both PCI effects, that is, level broadening as well as energy shift [8]. We propose, therefore, that PCI profiles from very short-lived core levels of adsorbates contain information on the dynamics of this screening process. Because of the small ionization cross sections of such levels [9] and the large widths of their spectral lines [10], related experiments are difficult, which is probably the reason why no successful attempts have been made so far. Access to the dynamics of more complex satellites or to that of matrix-induced energy losses like plasmons or electron-hole excitations will be even more difficult to observe without the use of true attosecond metrology.

There is, however, an interesting exception. The spin-dependent screening dynamics of magnetic impurities in 3d ferromagnets have been successfully investigated by inelastic resonant Raman scattering (IRRS) [11]. Using the lifetime of the 2p core holes as a time ruler (see the description of the core hole clock method below), magnetic screening time constants ranging from 1.5 fs for Ni to less than 180 as for Fe have been obtained [11].

22.2.2

Charge Transfer Dynamics and Resonant Photoemission

Lifetimes of inner shell levels can be very short. For those with large binding energies or those decaying via Coster–Kronig or super-Coster–Kronig processes, lifetimes are

well below 1 fs (see Ref. [10] for a compilation). Lifetime-broadened maxima are observed in kinetic energy spectra for the photoelectrons as well as for the decay (Auger) electrons. We note, however, that these homogeneous broadenings are correlated. For all decay processes with a final state of well-defined energy (e.g., the ground state of a doubly charged ion) and no further inelastic channels, energy conservation can only be violated for the (short) lifetime of the intermediate core-ionized state; it has to apply between initial (ground) and final (doubly ionized) states. In other words, a positive energy shift ($+\Delta E$) of the photoelectron is compensated by $-\Delta E$ of the decay electron. It has been convincingly demonstrated by coincidence experiments that excitation and de-excitation are coherent processes [12]. Unfortunately, coincidence experiments are very difficult to carry out, due to the very large background counts from solids. It is much easier to start with a *bound core resonance* instead and excite it with narrowband radiation. If the resonantly excited electron does not exchange energy with its environment during the lifetime of the core hole, which is typically the case for an isolated particle, due to energy conservation the energy of the decay electron (or decay photon) disperses linearly with the excitation energy. The decay electron spectrum resembles the off-resonant photoemission spectrum, with one-hole states (participator lines, corresponding to the main line in photoemission) and one-hole two-electron states (spectator lines, corresponding to shake-up satellites), however with (often very) different relative amplitudes [13]. For molecules, which may be vibrationally excited in the intermediate as well as in the final states, this dispersion rule holds strictly only within one set of vibrational quanta [13]; interesting redistribution processes among the vibrations are observed by detuning the initial excitation within the resonance. This coherent process, which is termed resonant photoemission or Auger resonant Raman effect (ARRE), is – besides other interesting applications in molecular physics – also a very powerful tool for investigation of ultrafast charge delocalization dynamics on surfaces [14–16].

Particles bound to surfaces or other molecules are not isolated. They can exchange charge and energy. If the status of the resonantly excited electron is changed during the lifetime of the core hole by interaction with the environment, the coherence of excitation and deexcitation noted above is lost. Particularly, delocalization of the resonance electron into a continuum, for example, into unoccupied electronic states of the substrate, converts the shape of the decay spectrum from resonant into normal Auger (Figure 22.1).

In many cases, both contributions can be well separated. Combined with the known lifetime of the core hole, the ratio of the integrated intensities of these two channels yield the charge delocalization time:

$$\tau_{\text{delocalization}} = \tau_{\text{core hole}} \cdot \frac{I_{\text{resonant}}}{I_{\text{nonresonant}}},$$

that is, $\tau_{\text{delocalization}}$ is measured in units of $\tau_{\text{core hole}}$ [14]. The CHC method looks at processes that are different from those observable by lasers in the optical range, but it also has some clear limitations. A fundamental complication is that the

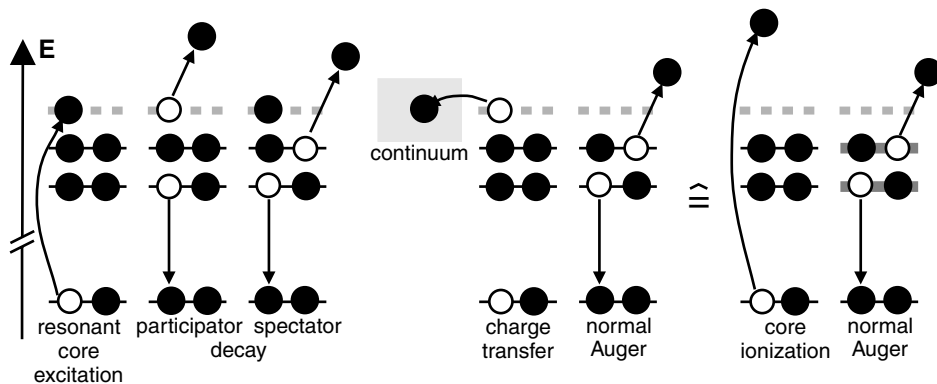


Figure 22.1 Charge delocalization measured by the core hole clock method. Inner shell levels and occupied outer shell/valence levels are indicated as solid black lines and unoccupied levels as dashed gray lines. Core excitons (left) decay via participator or spectator processes if the lifetime of the resonance is longer than

the lifetime of the core hole. If the delocalization of the resonantly excited electron, that is, its transfer to a continuum, for example, into unoccupied levels of the substrate, is faster than core decay, normal Auger is observed (middle) as for primary core ionization (right).

core ionization increases the effective atomic number from Z to $Z + 1$ and therefore changes the chemical behavior of the atom during the lifetime of the core hole (“equivalent core approximation” [1]). The excited electron whose transfer is observed is therefore initially localized on the atom with the core hole, while for laser excitation in the optical range, the electron wave packet is delocalized in the adsorbate layer, and the hole is in the substrate. This does not necessarily mean that one method, either the CHC or the optical laser pump–probe, provides a more accurate depiction of the systems dynamics. In fact, in the case of the CHC, the clear initial localization may well be closer to actual charge transfer processes, but these differences must be taken into account in interpretation and comparison. A severe limitation is that core levels of appropriate lifetime [10] may not be available for the surface particles of specific interest, or that the resonance energy may not be suitable for such measurements [14]. In addition, in molecular adsorbates with spatially extended valence state wave functions, it is difficult to distinguish intramolecular charge delocalization from heterogeneous electron transfer, without further geometrical and/or energetic information. Finally, the CHC method supplies only a number, namely, the ratio of both channels, albeit as a function of energy through the resonance, but this number does not yield information about the temporal evolution of the charge distribution. We will show that future experiments with attosecond pulses can avoid these limitations. We finally note that extracting charge delocalization times simply from the widths of resonance lines fails in most cases because other effects, particularly from inhomogeneity of the samples and also from vibrational envelopes, will cause additional line broadening, which in most cases cannot be discriminated from the lifetime effect, even by sophisticated data evaluation.

22.2.3

Scattering Experiments and Band Structure Buildup

Atomic and molecular orbitals of particles condensed into the solid-state interact, forming energy bands with energy values dependent on electron momentum. However, as for the collective behavior in the screening example, a few scattering events are necessary for the electrons to probe the structure of their environment in order to form bands. On a very short timescale, we can assume that the electrons “do not know” about the solid structure or the corresponding electronic band structure. This is confirmed by theoretical investigations and experiments on charge transfer during scattering of fast ions at surfaces. Neutralization of negative ions probes the unoccupied, while that of positive ions the occupied density of states at the surface. For crystalline materials, the density of states varies strongly with energy showing maxima, minima, and gaps. As a result, charge transfer rates should vary depending on the energetic positions of the projectile ionization or affinity levels and indeed such effects have been found using the CHC method outlined above [14]. Theory [17, 18] and experiment [18] show that the signature of the band structure in the charge transfer rates vanishes for increasing particle energies, corresponding to decreasing interaction times. We will see that this aspect is also of fundamental importance for experiments with attosecond light pulses and their interpretation.

22.3

Attosecond Experiments at Surfaces

22.3.1

General Remarks

The measurement of attosecond dynamics relies on the reproducible generation of events with attosecond duration and on probing techniques with commensurate resolution [19]. Until recently, the briefest reproducible events have been pulses of near-infrared (NIR) laser light, with durations of around 5 fs [20, 21]. At present, high-energy NIR pulses as short as 3.4 fs can be produced [22]. Traditionally, the fastest measurement techniques have used the envelope of these laser pulses for sampling [23]. However, these techniques have not yet been capable of resolving the time structure of subfemtosecond transients.

With the arrival of isolated attosecond pulses in the extreme ultraviolet (XUV) [24–27] and of carrier-envelope phase-stabilized intense few-cycle laser pulses [28], an apparatus was developed allowing reconstruction of atomic processes with a time resolution within the Bohr orbit time of ~ 150 as. In this apparatus, an accurately controlled few-cycle wave of visible light is used to collect “tomographic images” of the time–momentum distribution of electrons ejected from atoms following sudden excitation, for example, by XUV pulses of attosecond duration. From these images, the temporal evolution of both the emission intensity and initial momentum of

released electrons can be retrieved on a subfemtosecond timescale. As a first application, primary photo and secondary Auger electrons were probed. In general, transients can be triggered by an isolated attosecond electron or photon burst synchronized with the probing light field oscillations.

22.3.2

Principles of Surface-Related Attosecond Metrology

The technique draws on the basic operation principle of a streak camera [29–33]. Deflection of the electrons in a rapidly varying electric field allows reconstruction of the temporal profile of the electron bunch. In our case, the intense few-cycle pulse of a laser supplies this field (see below). By measuring the evolution of the emission intensity and momentum distribution of photoelectrons, this attosecond transient recorder (ATR) [34] has already provided insight into the temporal rearrangement of the electronic shell of excited atoms on a subfemtosecond scale. This technique has now been extended to the investigation of solid surfaces.

22.3.3

Generation of Isolated Attosecond Pulses and Principle of Attosecond Spectroscopy of Solids

In a gas target, the electric field of intense linearly polarized femtosecond laser pulses induces – in a highly nonlinear interaction – gigantic dipole oscillations by pulling an electron out of the atom and subsequently forcing it back toward the core in the next half-cycle of the electric field. These oscillations contain high-frequency components extending into the extreme ultraviolet and soft-X-ray regimes [20]. In a long laser pulse containing many field oscillation cycles, the giant dipole oscillations are repeated quasiperiodically, resulting in the emission of a series of high-energy bursts of subfemtosecond duration that appear in the frequency domain as high-order harmonics of the drive laser. In contrast, for an ultrashort few-cycle laser pulse, only a few dipole oscillations can occur, and furthermore these few oscillations vary strongly in amplitude. The field oscillation with the largest amplitude produces a single burst of radiation in the spectral range of the highest emitted photon energies [35].

With waveform-controlled few-cycle laser pulses [28], the giant atomic dipole oscillations can be precisely controlled and reproduced from one laser shot to the next. As a result, the XUV burst parameters, including duration, energy, and timing with respect to the laser field, are well reproduced from one shot to the next. Because the XUV burst is precisely synchronized to the field oscillations of the driving laser pulse, we can use the XUV burst *in combination with* the oscillating laser field for attosecond spectroscopy. This is essential, as these laser-produced XUV bursts are currently too weak to be used for *both* triggering *and* probing electron dynamics. Instead, the oscillating laser field, which changes its strength from minimum to maximum within only ~ 1200 as for a wavelength of 750 nm, must take the role of the probing attosecond pulse. Experiments have proven that precise control over the

waveform of few-cycle laser pulses makes it possible to *control* and *observe* atomic processes on a subfemtosecond timescale.

Corkum and coworkers [32] proposed the basic concept of ATR metrology in 2002, which was further developed with a comprehensive quantum theory by Brabec and coworkers [33]. Today, ATR based on photoemission from noble gases is an established technique for characterizing the duration of attosecond XUV pulses [22, 34, 36]. The principle of ATR is based on generating a photoelectron by an attosecond XUV burst in the presence of an intense, linearly polarized, few-cycle laser field $E_L(t) = E_0(t)\cos(\omega_L t + \varphi)$. The momentum of the released electrons is changed by $\Delta p = eA_L(t)$ along the laser field vector, where $A_L(t_r) = \int_{t_r}^{\infty} E_L(t)dt$ is the vector potential of the laser field, e stands for the rest mass of the electron, and t_r is the instant of release of the photoelectron. This momentum transfer Δp maps the temporal profile of the electron emission onto a similar distribution of final momenta $p_f = p_i + \Delta p$ within a time window of $T_0/2 = \pi/\omega_L$. If the electron's initial momentum p_i is constant in time and their emission terminates within $T_0/2$, the temporal evolution of the electron emission can be unambiguously retrieved from a single "streaked" momentum distribution.

In the case of multiple, distinct emission lines in the photoelectron spectrum, the ATR can be used to compare the characteristics of the photoelectrons originating from the different states. For example, the photoelectron spectrum of a (110)-oriented tungsten surface obtained with the attosecond XUV pulses (Figure 22.2) shows two distinct peaks originating from 5d/6sp valence band electrons and 4f/5p core levels. By employing the ATR, the relative timing of the photoelectrons emerging through the surface can be determined. As illustrated in Figure 22.3, photoelectrons traversing the surface at different instants of time are subject to different phases of the streaking field. It is possible to extract an effective emergence time of the electrons using the waveform-controlled streaking field even though it penetrates the bulk due to the optical index of refraction. As a result, the effective delay in photoemission can be reconstructed from the spectrograms.

22.3.4

Hardware Requirements

At present, solid-state and surface experiments are performed in an attosecond beamline consisting of a HHG generation chamber, an XUV spectrometer, and several differential pumping stages in order to ensure UHV vacuum conditions in the measurement chamber. The measurement chamber contains a two-part multi-layer mirror for the XUV and IR pulses as described in Ref. [23]. The mirror acts as a spectral filter for the generation of single, isolated attosecond pulses from 80 to 300 as duration and is – with its two parts – used to introduce the temporal delay between the XUV and the IR pulses. Emitted electrons are recorded with a time-of-flight spectrometer. The analyzer section of the measurement chamber is rotatable, allowing independent settings of the angles of detection and light incidence; the latter is important to meet the Brewster criterion for the NIR, which minimizes the effect of the phase-shifted reflected wave in the streaking experiment. The sample is

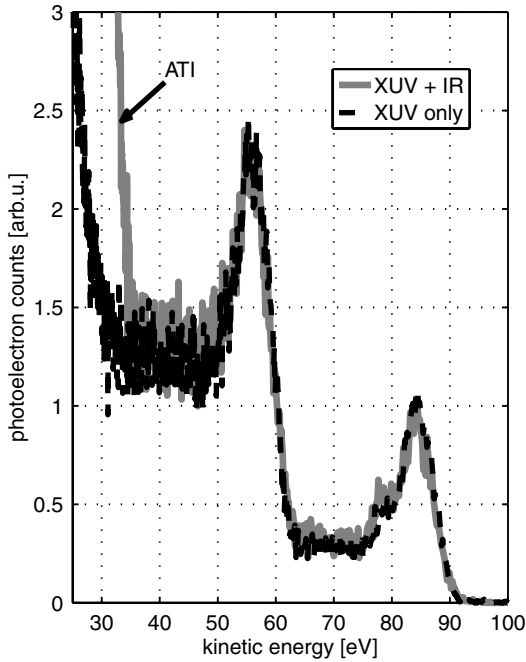


Figure 22.2 Raw photoelectron spectra of tungsten (110) measured with (gray curve) and without (dashed black curve) the presence of the probe NIR streaking field using XUV photons of ~ 91 eV. The spectra show two distinct peaks originating from 5d/6sp valence

electrons and 4f/5p core levels at ~ 83 and ~ 56 eV, respectively. In the presence of the NIR probe field, there is an intense photoelectron signal below 35 eV induced by above-threshold ionization (ATI). Each spectrum was obtained by integration over 60 000 laser pulses.

mounted on a manipulator that moves it between the measurement chamber and a separate preparation chamber for cleaning, conditioning, and characterization purposes.

22.3.5

First Experimental Results

A tungsten (110) surface was the sample used in the first proof-of-principle experiments [38]. From clean W(110), two parallel spectrograms are observed that originate from different electronic states, 5d valence and 6sp conduction band electrons, and 4f, 5p core electrons, which are emitted with different kinetic energies (Figure 22.4a). The large bandwidth of the excitation pulse does not allow separation of the 4f/5p and the 5d/6sp intensities, respectively. But due to their comparatively small ionization cross sections and densities of states, the 5p and 6sp contributions are minor and the two emission peaks are dominated by 5d valence and 4f core contributions, respectively. Both spectrograms show the change in electron energy corresponding to the evolution of the electric field of the NIR streaking pulse. Figure 22.4b shows a

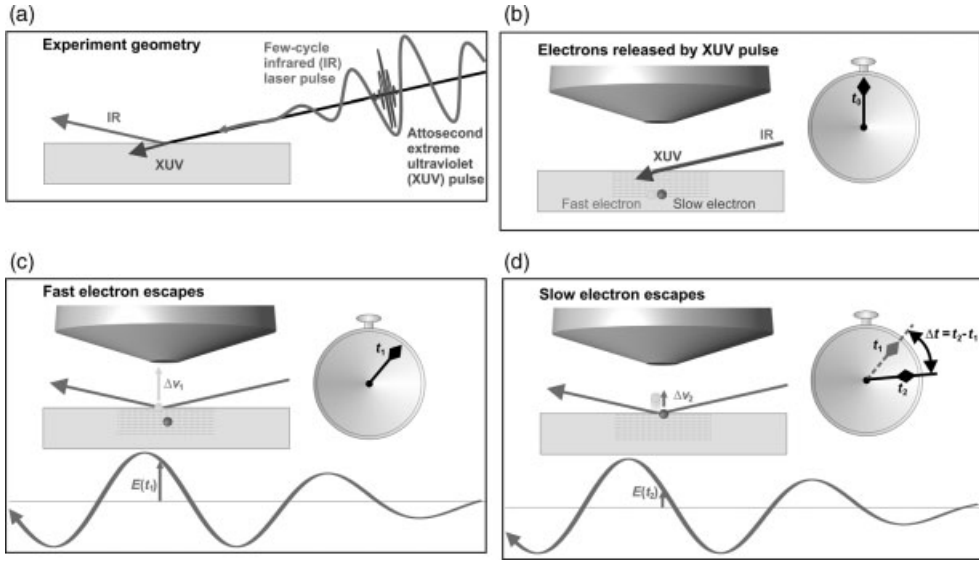


Figure 22.3 Attosecond spectroscopy on solids: Electrons arriving at the surface at different instants of time are subject to different phases of the streaking field outside the metal. (In this figure, we neglect the streaking field inside the solid, which due to the metal’s optical properties is weak.) In panel (a), an isolated attosecond XUV pulse and a delayed few-cycle waveform-controlled streaking field are incident on a solid surface. In panel (b), at time t_0 , the XUV pulse is absorbed in the solid and two types of photoelectrons are born, for simplicity one photoelectron is called “slow” and the other “fast.” In panel (c), at time t_1 , the fast electron has propagated to the surface and is now subject to the strong streaking field, which modulates its outgoing kinetic energy

depending on the instant of release. In panel (d), at time t_2 , the slow electron has reached the surface and feels the strong streaking field at the vacuum side; since it has emerged at a different time, the modulation of its kinetic energy will vary depending on the precise delay in emission. By evaluation of the full streaking spectrograms, collected as a function of relative delay between the attosecond XUV pulse and the streaking field, the delay in photoemission can be determined. Compared to streaking experiments at isolated particles, detailed models of electron localization, and electron and photon transport and interaction are necessary for the evaluation of such spectrograms.

center-of-mass (COM) analysis of the spectrograms. For this analysis, the time-dependent COM of both emission lines were calculated in a global fit by

$$\text{COM}_{\text{CB}}(t) = a_1 e^{-4\ln(2)\frac{(t-t_0)^2}{\text{FWHM}^2}} \sin(\omega t + \phi_0) + \text{offset}_{\text{CB}},$$

$$\text{COM}_{\text{4f}}(t) = a_2 e^{-4\ln(2)\frac{(t-t_0-\Delta t)^2}{\text{FWHM}^2}} \sin(\omega t + \phi_0 - \omega \Delta t) + \text{offset}_{\text{4f}},$$

where a_1 , a_2 , $\text{offset}_{\text{CB}}$, and $\text{offset}_{\text{4f}}$ denote the streaking amplitudes and the time-independent positions of the emission lines, respectively. t_0 and FWHM denote center and full width at half maximum of the Gaussian-shaped envelope of the streaking field, and ϕ_0 gives its carrier envelope phase. The parameter Δt accounts for

a temporal shift between the spectrograms of both emission lines. The fit results are shown as solid lines in Figure 22.4b and a temporal shift in the streaking of 85 ± 35 as corresponding to the same delay in emission of the photoelectrons from the tungsten surface is extracted. This result is in good agreement with the initial study, where the valence electrons were found to be emitted approximately 100 as earlier than their tightly bound core-state counterparts [38].

These results demonstrate the technical capability of measuring photon-induced electron release, electron transport through the topmost atomic layers of a solid sample, and emission into the vacuum in real time, with attosecond temporal resolution. However, explaining the state-dependent differences of these emission dynamics as seen in the streaking experiment is, unfortunately, a much more challenging task than its equivalent for isolated particles [34]. Four different theoretical approaches to describe the dynamics seen in this W(110) experiment exist so

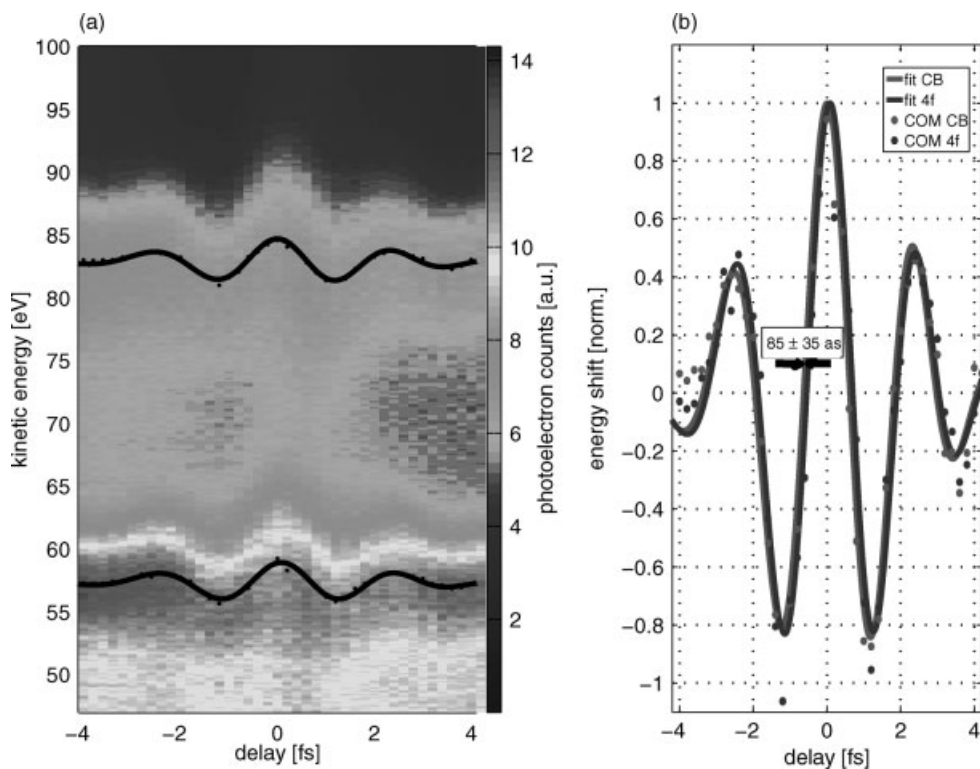


Figure 22.4 (a) Raw ATR spectrogram of a tungsten (110) surface. Photoelectron intensities are given in arbitrary units. The 5d/6sp and 4f/5p peaks are fitted with a Gaussian function and the peak positions at every time point are indicated by dots. The solid line shows the transient shifts of these peaks as obtained

from a global fit equivalent to the center-of-mass (COM) analysis. (b) COM analysis of the spectrogram. The COM of both emission lines as measured are given as dots, a global fit to both COM traces is shown in solid lines. See text for details. (Please find a color version of this figure on the color plates.)

far, all yielding delayed emission of the core versus valence electrons from 42 to 110 as. The first theoretical approach by Echenique and coworkers explained the delayed emission of the core electrons by different group velocities of the final states [38]. Assuming validity of the static band structure picture, the authors showed that for the photon energy of the experiment (91 eV), the final state bands of the valence electrons exhibit stronger dispersion than those of the core electrons. As a result, a smaller effective mass, larger group velocity, and more rapid transport were concluded for the valence electrons, explaining the observed timing. A critical point of this model was the application of the static band structure. As indicated in the introduction, at least a few scattering events are expected to be required for the formation of delocalized states, and attosecond time intervals may be too short for these processes to occur. Considering this, Kazansky and Echenique have investigated in a second study the relative contributions of final and initial state effects to the observed dynamics [39]. In their revised quantum model, they treat the core electrons as localized and the valence electrons as completely delocalized. Attenuation by inelastic scattering is taken into account as well as electron–hole interaction for the inner shell levels, but not for the valence states. The streaking field inside the metal is assumed to be zero. Pseudopotentials obtained for copper are used to model electron transport. Calculations based on this one-dimensional theory also reproduce the experimentally obtained result quite well. Compared with the first approach, however, the relative magnitudes of final and initial state effects are reversed. The authors show that different final state energies contribute only a Δt of 10 as to the total delay; the main effect can now be attributed to the localized nature of the core electrons in contrast to the valence electrons that are treated as delocalized.

A third study by Zhang and Thumm also assumes localized core and delocalized valence electrons in the jellium approximation [40]. Compared to Ref. [39], the authors include the streaking field inside the solid: they argue that the skin depth (~ 100 Å) is much larger than the electron's mean free path (~ 5 Å). While the effect of streaking is treated nonperturbatively, the photoemission by the XUV pulse is treated by first-order perturbation theory. The authors introduce interfering contributions from different lattice layers to the photoemission dipole matrix element for the localized core states but not for the valence states, which according to their assumption are completely delocalized (jellium approximation). According to their model, this interference is the main source for the delayed emission of the 4f core electrons. For this delay they obtain 110 as, a value compatible with the experiment.

A fourth theoretical study by Lemell *et al.* models the attosecond streaking experiment by classical transport [41]. Quantum effects enter this classical calculation via a stochastic force $F_{\text{stoc}}(t)$ containing elastic and inelastic scatterings with tungsten cores, as well as with conduction electrons. Other forces changing the electron's momenta result from the NIR streaking field, which penetrates ~ 85 layers of the solid in their model, and from the potential barrier at the surface. Rather detailed assumptions are made concerning the properties of the various involved electronic states. They discriminate 5p and 4f core electrons and 5d and 6s valence electrons, and treat only the 6s band as delocalized. Elastic scattering cross sections are calculated with the ELSEPA package [42]. Inelastic scattering cross sections and

angular distributions of inelastically scattered electrons are obtained from the momentum distribution and energy-dependent dielectric constant of tungsten. Two limiting cases are considered for the final states: (a) a free particle dispersion relation and (b) the group velocity distribution of Silkin *et al.* (Ref. [38], supplementary material). Depending on these two alternatives, delayed emission of the core electrons from 42 (case a) to 110 as (case b) is obtained; the authors point out, however, that the group velocity distribution from Ref. [38] had to be blueshifted by 8 eV to obtain the maximum effect. For the limiting case (a), larger emission depth of the core electrons and the valence electrons scattered inelastically into the energy region of the core photoelectrons are the main sources of the observed delay. We note that the authors address possible extensions of their model, particularly inclusion of local field enhancements at the surface (plasmons), which might affect emission and transport of localized and delocalized states differently.

22.3.6

Future Experiments

22.3.6.1 Improving the Theoretical Description of Streaking Experiments on Solid Targets

The fact that four different theoretical approaches based on rather different assumptions yield contradicting explanations for the experimentally observed electron emission dynamics from a metal surface, yet numerical values for the expected delay, which all are within the experimental scatter, clearly indicates that the streaking process at solid surfaces is not well understood. Many processes and properties, such as primary photoemission, screening by itinerant electrons, transport, including elastic and inelastic scatterings in the bulk and across the solid/vacuum interface, the influence of the streaking field inside the material, and the localization of the individual electronic states contribute to the effect. Future experiments must help to solve this puzzle. A homogeneous sample like tungsten with its overlapping localized (5d) and delocalized (6sp) valence electrons and core levels of different symmetry (5p, 4f) that are energetically not resolvable under the conditions of an attosecond photoemission experiment may be too complex for this purpose. Well-tailored samples and experiments performed on these samples with different photon energies are required to disentangle the individual contributions of the above processes to the overall delay observed in the experiment. Such samples could be thin crystalline layers heteroepitaxially grown on top of substrates from different materials (Figure 22.5).

By varying thickness and elemental composition of these layered samples, transport and electronic properties could be varied independently and disentangled. Experiments with different photon energies would test the influence of final state effects.

22.3.6.2 Dynamics of Band Structure Formation, Screening, and Magnetic Effects

It is clear from the considerations given above that a comprehensive description of the streaking process must encompass information about the dynamics of band

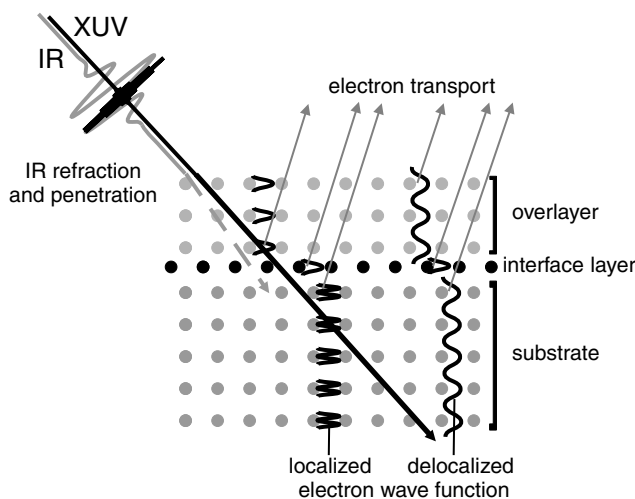


Figure 22.5 Sketch of an exemplary future sample design. Achieving a better understanding of the streaking process requires discriminating the influences of electron localization, electron transport surface and interface barriers, and refraction and penetration of the IR streaking field. Appropriately tailored crystalline sandwich structures of different materials, metallic and insulating, can help to solve this task.

structure formation and screening. To attain this, it will be particularly important to compare experiments with different photon energies, resulting in electron propagation in different final states, with different effective masses in the static band structure picture. We expect the maximum contrast for flat final states, for example, states with d or f symmetry, where the deviation from free particle dispersion is largest. Exciting electrons into such states, while varying the duration of the time interval during which the photoemission process occurs by tuning the spectral width of the XUV pulse, could reveal the transition from the free particle (for short pulses) to the static band regime (for long pulses), similar to the variation of the projectile energy in ion scattering experiments mentioned in Section 22.2.3.

On a short timescale, the concept of screening encompasses scattering and redistribution of electrons, and as such its dynamics must enter a detailed theory of streaking, as does that of the dynamics of band formation. Following the considerations above, well-designed samples can help to isolate the related phenomena. For many materials, photoemission is accompanied by simultaneous excitation of intrinsic plasmons, that is, collective excitations of the electron gas. Because of their many-body character, time for at least a few scattering events is required for their formation. A goal of future experiments will be the investigation of the emission dynamics of plasmon satellites and of features resulting from the inelastic electron-hole excitations. We also expect attosecond-related deviations from the static picture in line shape and line energy for polarization screening of photoemission from adsorbates, for example, from inert layers like monolayers of rare gases, and for charge transfer screening satellites in photoemission from

compounds, for example, Mott insulators like nickel oxide. Of particular interest will be the class of valence band screening satellites obtained for 3(4,5)d transition metals, 4f rare earth metals, and 5f actinides. For these materials, vacancies in the 3(4,5)d or 4(5)f shells can be screened either by localized d or f electrons or by delocalized conduction electrons [1]. The latter screening process is less efficient, leading to photoemission satellites with binding energies larger than that of the main line by a few eV. It is of particular interest that these satellites can also be resonantly excited by the decay of [3(4,5)p]3(4,5)d or [4(5)d]4(5)f transitions, giving rise to interference between direct photoemission (with different screening scenario) and autoionization channels with emission delayed by the lifetime of the core hole. It is clear that by varying the material, the thickness of the active material (by layered samples), the photon energy, and the XUV pulse duration that many routes to study these different processes selectively will be opened. In particular, analysis of the temporal evolution of Fano line profiles resulting from interference phenomena will exclusively be possible with the attosecond spectroscopy approach [43].

The investigation of ultrafast magnetic phenomena is another field that has attracted considerable interest during the last years. Recently, coherent coupling of the polarization induced by the photon field of a femtosecond laser pulse with the spins of ferromagnetic samples has been demonstrated [44]. The origin of this coupling mechanism has been explained by relativistic quantum electrodynamics, beyond the spin-orbit coupling involving the ionic potential [44]. Intense, few-cycle IR pulses in combination with ultrashort XUV probe pulses and spin-sensitive detection will enable the investigation of such ultrafast magnetic phenomena with unprecedented temporal resolution. These studies will also include the microscopic details of the incoherent thermalization of excited spin and allow comparison with the corresponding charge processes.

22.3.6.3 Charge Transport

Ultrafast charge transport and adsorbate-to-substrate charge transfer are processes of key importance for the dynamics of bond formation and bond breaking, modification of materials by electronic excitations, electrochemistry, including processes in dye-sensitized solar cells, spectroscopy, and molecular electronics. The core hole clock method has clear limitations, as mentioned in Section 22.2.3. In particular, it is not possible to follow the evolution of the charge distribution in real time. Attosecond streaking, however, can achieve this task. After a resonant inner shell excitation by an attosecond XUV pulse, it can follow the entire evolution of the charge redistribution, starting with autoionization spectra immediately after excitation and ending with nonresonant core decay after complete charge delocalization. This transition between the two regimes will be evident in both the energetics and the line shapes of the streaking spectrogram of the decay electrons. This method will reach its full potential as soon as the XUV photon energies in the K-shell excitation region of the chemically important elements C, N, and O become available (from 280 to 540 eV).

All the experiments mentioned so far, apart from the magnetization studies, are common in that the excitation does not disturb the system under investigation. That

is, the excitation does not drive the population of states far from equilibrium, as is the case, for example, in classical pump–probe experiments with femtosecond laser. At present, the intensity of the attosecond XUV pulses is too low to promote a large enough fraction of electrons into an excited state to be probed by a subsequent laser pulse.

Once they become feasible, such pump–probe experiments, with two attosecond pulses, will be powerful despite their perturbative nature. The second pulse could be used for ultrafast time-resolved XPS, where time-dependent chemical shifts would make it possible to monitor the electronic system's evolution. Tracer atoms with well-separated spectral features along the trajectory of charge transport would allow a site-selective view. At present, this detection scheme is applicable only for excitation with (low) harmonics of the NIR pulse. Despite these limitations, it is an extremely promising approach. The progress in light wave synthesis will enable detailed control of pulse shapes in time, making excitation of selected electronic states possible by coherent control of electron wave packets, the motion of which can then be followed by time-resolved XPS. We foresee for this method a level of potential comparable to multipulse NMR, which has revolutionized stereochemistry. We expect an analogous impact on the investigation of electron dynamics in solids and at interfaces and all related phenomena.

Acknowledgments

Help during the experiments by N. Müller, E. Magerl, S. Neppel, M. Stanislawski, E. Bothschafter, and N. Karpowicz is gratefully acknowledged. We thank Martin Wolf for helpful discussions. We gratefully acknowledge support by the Deutsche Forschungsgemeinschaft through the Excellence Cluster Munich Center for Advanced Photonics, Research Area A1 and C1. R.K. acknowledges support from the Sofja Kovalevskaja Award by the Alexander-von-Humboldt Foundation and the ERC Starting Grant.

References

- Hüfner, S. (2003) *Photoelectron Spectroscopy*. Springer, Berlin, and references therein.
- Shirley, D.A. (1972) *Chem. Phys. Lett.*, **16**, 220; Gelius, U. (1974) *J. Electron Spectrosc.*, **5**, 985.
- Manne, R. and Åberg, T. (1970) *Chem. Phys. Lett.*, **7**, 282.
- Chiang, T.C., Kaindl, G., and Mandel, T. (1986) *Phys. Rev. B.*, **33**, 695.
- Borisov, A., Sánchez-Portal, D., Díez Muiño, R., and Echenique, P.M. (2004) *Chem. Phys. Lett.*, **397**, 95.
- Huber, R., Tauser, F., Brodschelm, A., Bichler, M., Abstreiter, G., and Leitensdorfer, A. (2001) *Nature*, **414**, 286.
- Thomas, T.D., Hall, R.I., Hochlaf, M., Kjeldsen, H., Penent, F., Lablanquie, P., Lavollée, M., and Morin, P. (1996) *J. Phys.*, **B29**, 3245.
- Kassühlke, B., Romberg, R., Averkamp, P., and Feulner, P. (1998) *Phys. Rev. Lett.*, **81**, 2771.
- Yeh, J.J. and Lindau, I. (1985) *Atom. Data Nucl. Data Tables*, **32**, 1.

- 10 Campbell, J.L. and Papp, T. (2001) *Atom. Data Nucl. Data Tables*, **77**, 1.
- 11 Braicovich, L. and van der Laan, G. (2008) *Phys. Rev.*, **B78**, 174421, and references therein.
- 12 Jensen, E., Bartynski, R.A., Hubert, S.L., Johnson, E.D., and Garrett, R. (1989) *Phys. Rev. Lett.*, **62**, 71.
- 13 Gel'mukhanov, F. and Ågren, H. (1999) *Phys. Rep.*, **312**, 87; Piancastelli, M.N. (2001) *J. Electron Spectrosc.*, **107**, 1, and references therein.
- 14 Menzel, D. (2008) *Chem. Soc. Rev.*, **37**, 2212; Brühwiler, P.A., Karis, O., and Mårtensson, N. (2002) *Rev. Mod. Phys.*, **74**, 703, and references therein.
- 15 Föhlisch, A., Feulner, P., Hennies, F., Fink, A., Menzel, D., Sanchez-Portal, D., Echenique, P.M., and Wurth, W. (2005) *Nature*, **436**, 373; Deppe, M., Föhlisch, A., Hennies, F., Nagasono, M., Beye, M., Sanchez-Portal, D., Echenique, P.M., and Wurth, W. (2007) *J. Chem. Phys.*, **127**, 174708.
- 16 Wurth, W. and Menzel, D. (2000) *Chem. Phys.*, **251**, 141.
- 17 Borisov, A.G., Kazansky, A.K., and Gauyacq, J.P. (1998) *Phys. Rev. Lett.*, **80**, 1996; Borisov, A.G., Kazansky, A.K., and Gauyacq, J.P. (1999) *Phys. Rev.*, **B59**, 10935.
- 18 Canário, A.R., Borisov, A.G., Gauyacq, J.P., and Esaulov, V.A. (2005) *Phys. Rev.*, **B71**, 121401(R).
- 19 Zewail, A. (2000) *J. Phys. Chem.*, **A104**, 5660–5694.
- 20 Brabec, T. and Krausz, F. (2000) *Rev. Mod. Phys.*, **72**, 545–591.
- 21 Keller, U. (2003) *Nature*, **424**, 831–838.
- 22 Goulielmakis, E. et al. (2008) *Science*, **320**, 1614.
- 23 Drescher, M. et al. (2001) *Science*, **291**, 1923–1927.
- 24 Paul, P.M., Toma, E.S., Breger, P., Mullot, G., Augé, F., Balcou, Ph., Muller, H.G., and Agostini, P. (2001) *Science*, **292**, 1689–1692.
- 25 Mairesse, Y. et al. (2003) *Science*, **302**, 1540–1543.
- 26 Tzallas, P. et al. (2003) *Nature*, **426**, 267–271.
- 27 Hentschel, M. et al. (2001) *Nature*, **414**, 509–513.
- 28 Baltuska, A. et al. (2003) *Nature*, **421**, 611–615.
- 29 Wheatstone, C. (1835) *Philos. Mag.*, **6**, 61.
- 30 Bradley, D.J., Liddy, B., and Sleet, W.E. (1971) *Opt. Commun.*, **2**, 391.
- 31 Schelev, M. et al. (1971) *Appl. Phys. Lett.*, **18**, 354.
- 32 Itatani, J. et al. (2002) *Phys. Rev. Lett.*, **88**, 173903.
- 33 Kitzler, M., Milosevic, N., Scrinzi, A., Krausz, F., and Brabec, T. (2002) *Phys. Rev. Lett.*, **88**, 173904.
- 34 Kienberger, R. et al. (2004) *Nature*, **427**, 817–821.
- 35 Christov, I.P., Murnane, M.M., and Kapteyn, H.C. (1997) *Phys. Rev. Lett.*, **78**, 1251–1254.
- 36 Goulielmakis, E. et al. (2004) *Science*, **305**, 1267.
- 37 Bandrauk, A.D. et al. (2004) *Int. J. Quantum Chem.*, **100**, 834; Niikura, H. et al. (2006) *Phys. Rev. A*, **73**, 021402; Yudin, G.L. et al. (2006) *Phys. Rev. A*, **72**, 051401.
- 38 Cavalieri, A.L. et al. (2007) *Nature*, **449**, 1029.
- 39 Kazansky, A.K. and Echenique, P.M. (2009) *Phys. Rev. Lett.*, **102**, 177401.
- 40 Zhang, C.-H. and Thumm, U. (2009) *Phys. Rev. Lett.*, **102**, 123601.
- 41 Lemell, C., Solleder, B., Tökési, K., and Burgdörfer, J. (2009) *Phys. Rev.*, **A79**, 062901.
- 42 Salvat, F., Jablonski, A., and Powell, C. (2005) *Comput. Phys. Commun.*, **165**, 157.
- 43 Wickenhauser, M., Burgdörfer, J., Krausz, F., and Drescher, M. (2005) *Phys. Rev. Lett.*, **94**, 023002.
- 44 Bigot, J.-Y., Vomir, M., and Beaurepaire, E. (2009) *Nat. Phys.*, **5**, 515; see also Bovensiepen, U. (2009) *Nat. Phys.*, **5**, 461.